
KERNEL DENSITY BAYESIAN INVERSE REINFORCEMENT LEARNING

A PREPRINT

Aishwarya Mandyam

Department of Computer Science,
Stanford University,
Gladstone Institutes
am2@stanford.edu

Didong Li

Department of Biostatistics
University of North Carolina at Chapel Hill
didongli@unc.edu

Diana Cai

Department of Computer Science
Princeton University
dcai@cs.princeton.edu

Andrew Jones

Department of Computer Science
Princeton University
aj13@princeton.edu

Barbara E. Engelhardt

Gladstone Institutes
Department of Biomedical Data Science
Stanford University
bengelhardt@stanford.edu

March 14, 2023

ABSTRACT

Inverse reinforcement learning (IRL) is a powerful framework to infer an agent’s reward function by observing its behavior, but IRL algorithms that learn point estimates of the reward function can be misleading because there may be several functions that describe an agent’s behavior equally well. A Bayesian approach to IRL models a distribution over candidate reward functions, alleviating the shortcomings of learning a point estimate. However, several Bayesian IRL algorithms use a Q -value function in place of the likelihood function. The resulting posterior is computationally intensive to calculate, has few theoretical guarantees, and the Q -value function is often a poor approximation for the likelihood. We introduce kernel density Bayesian IRL (KD-BIRL), which uses conditional kernel density estimation to directly approximate the likelihood, providing an efficient framework that, with a modified reward function parameterization, is applicable to environments with complex and infinite state spaces. We demonstrate KD-BIRL’s benefits through a series of experiments in Gridworld environments and a simulated sepsis treatment task.

1 Introduction

Reinforcement learning (RL) methods find policies that maximize an agent’s long-term expected reward within a Markov decision process (MDP). In many observational data settings, we observe a sequence of states and actions for an agent carrying out a policy driven by an unknown reward function. It can be useful to learn this reward function to identify the factors driving the agent’s behavior. For example, in a hospital setting, we see a patient’s treatment schedule and measurements of physiological state. To make sense of the underlying factors influencing treatment decisions, we can identify the clinician’s reward function (i.e., objectives), and examine how this function drives treatment decisions given a patient’s state. It is particularly difficult to infer the reward function in this setting because the vector of observed covariates for a patient at a given time is often noisy and partially missing, and there may be several candidate reward functions that can explain the doctor’s behavior.

Inverse reinforcement learning (IRL) methods infer an agent’s reward function given observations of the agent’s behavior. Early IRL algorithms were used to identify point estimates of the reward function that best explained an agent’s behavior [2, 31], and were applied to problems in path planning [30], urban navigation [49] and robotics [24, 35]. A point estimate can also aid in imitation learning, where the inferred reward function is used to fit RL policies that replicate desired behavior.

Despite the success of early IRL approaches, there are limitations to inferring a point estimate. First, the IRL problem is often non-identifiable [2, 36, 49, 50], meaning there may be multiple (and possibly infinite) reward functions that explain a set of behaviors equally well. Second, for finite demonstration data, point estimates fail to capture the uncertainty and noise in the data-generating process. Thus, it is advantageous to take a Bayesian approach, which treats the reward function as inherently random and communicates a degree of uncertainty that relies on the dataset distribution. A Bayesian approach to IRL computes a posterior distribution that places mass on reward functions proportional to how well they explain the observed behavior [5, 13, 14, 27, 28, 34].

However, existing Bayesian IRL methods can be computationally demanding. In Bayesian modeling, likelihood specification has a large impact on the resulting posterior distribution. The formulation of the likelihood function (i.e., the function describing the probability of observing a state-action pair given a reward function) is unknown in the IRL setting. Existing approaches replace it with an optimal Q -value function, denoted by Q^* , which best approximates the long-term expected reward for a given state-action tuple ([34]). The Q -value function must be learned using Q -learning [42], a “forward RL” algorithm, or one that solves an environment’s MDP. The original algorithm pioneered by Ramachandran and Amir [34] and the majority of its successors use Markov chain Monte Carlo (MCMC) sampling to compute a posterior over the reward function, and every iteration of MCMC requires forward RL for each sampled reward function. This is computationally expensive, especially with infinite or high-dimensional state spaces. Additionally, a posterior that uses Q^* as a likelihood is equivalent to a Gibbs posterior [6, 47] and lacks desirable theoretical properties [6].

We address these challenges with kernel density Bayesian inverse reinforcement learning (KD-BIRL), a method that (1) estimates the likelihood function directly, leading to theoretical guarantees for the consistency of the resulting posterior distribution, and (2) disassociates the number of times forward RL is required from the number of iterations of MCMC sampling, thus reducing computational complexity. The contributions of our work are as follows:

1. We propose KD-BIRL, a Bayesian IRL method that uses conditional kernel density estimation to directly approximate the likelihood function (Section 3).
2. We justify our method theoretically by proving posterior consistency, and demonstrating that the posterior contracts to the equivalence class of the expert reward function (Section 4).
3. We show that KD-BIRL’s posterior estimates efficiently and accurately capture agent priorities in Gridworld environments (Section 5).
4. We demonstrate that, with a feature-based reward function, KD-BIRL can successfully infer rewards in complex state spaces such as a sepsis management task (Section 5).

2 Preliminaries

2.1 Background: Inverse reinforcement learning (IRL)

The goal of IRL methods is to infer the reward function of an agent, given its behavior. An RL agent interacts with and responds to an environment that can be defined using an MDP. An MDP is represented by $(\mathcal{S}, \mathcal{A}, P, R)$, where \mathcal{S} is the state space; \mathcal{A} is the set of actions; $P(s_{t+1}^e | s_t^e, a_t)$ defines state-transition probabilities from time t to $t + 1$; and $R : \mathcal{S} \rightarrow \mathbb{R}$ is a reward function, where $R \in \mathcal{R}$ and \mathcal{R} denotes the space of reward functions. The input to an IRL algorithm is a set of expert demonstrations, $\{(s_t^e, a_t^e)\}_{t=1}^n$, where each demonstration is a 2-tuple (s_t^e, a_t^e) representing an agent’s state and chosen action at time t . These demonstrations are assumed to arise from an agent acting according to policy, $\pi^* : \mathcal{S} \rightarrow \mathcal{A}$, that is optimal for a fixed but unknown reward function R^* . Given these demonstrations, IRL algorithms seek a reward function R^* such that π^* is optimal with respect to R^* .

Bayesian approaches to IRL treat the reward function R as inherently random. By specifying a prior distribution over R and a likelihood function for the observed data, these methods then infer a posterior distribution over R given n expert demonstrations of an agent $\{(s_i^e, a_i^e)\}_{i=1}^n$. Using Bayes rule, the posterior density is equivalent to the product of the prior distribution on the reward, $p(R)$, and the likelihood of the expert demonstrations given the reward function, with a normalizing constant that corresponds to the probability of the expert demonstrations:

$$p(R | \{(s_i^e, a_i^e)\}_{i=1}^n) = \frac{p(R) \prod_{i=1}^n p(s_i^e, a_i^e | R)}{p(\{(s_i^e, a_i^e)\}_{i=1}^n)}. \quad (1)$$

In the initial formulation of Bayesian IRL (BIRL) [34], the authors propose using a Q -value function to calculate the likelihood in Equation (1). The Q -value function for a given policy π at time t is $Q^\pi(s_t, a_t) = r_t + \gamma \mathbb{E}_{s' \sim P}[V^\pi(s')]$, where s_t, a_t , and r_t are the state, action, and reward at time t , and $\gamma \in [0, 1]$ is a discount factor. This approach uses an

optimal Q -value function, Q^* , as a component of the likelihood within a Gibbs posterior framework. The “likelihood” takes the form

$$p(s, a | R) \propto e^{\alpha Q^*(s, a, R)}, \quad (2)$$

where $Q^*(s, a, R)$ is the optimal Q -value function for reward function R , and $\alpha > 0$ is an inverse temperature parameter that represents confidence in the agent’s ability to select optimal actions.

There are several potential challenges with learning the aforementioned BIRL posterior. First, the optimal Q^* is found using Q -learning, a forward RL algorithm, and Q^* is typically expensive to estimate for a new R . BIRL uses MCMC, which requires learning Q^* on every iteration of sampling for a new R . In addition, because Equation 2 is a loss-based function (rather than a true likelihood), the resulting function is not a classical Bayesian posterior [40] and does not have theoretical guarantees regarding posterior contraction (more details in Appendix Section 2.3). Additionally, Q -value estimates can be incorrect for states that are very rarely visited, as often happens in infinite state spaces, leading to incorrect likelihood estimates that can affect the accuracy of the BIRL posterior.

2.2 Related Work

Several extensions to the original BIRL algorithm [34] have been proposed. The first set of methods identifies nonparametric reward functions [14, 15, 25, 32, 45]. These algorithms use a variety of strategies such as Gaussian processes [25, 32], Indian buffet process (IBP) priors [15], and Dirichlet process mixture models [14] to learn reward functions for MDPs with large state spaces that may include sub-goals. Other methods reduce computational complexity by using either more informative priors [38], different sampling procedures (e.g., Metropolis-Hastings [14] or expectation-maximization [48]), variational inference to approximate the posterior [13], or by learning several reward functions that each describe a subset of the state space [27, 28]. However, all of these approaches use a Q -value function in place of the likelihood and hence still suffer from consistency and computational issues; this construction is both inefficient and limits desirable Bayesian behaviors with regard to posterior sampling and uncertainty quantification.

To address these computational and consistency issues, it is necessary to either directly estimate the likelihood, reduce the number of times forward RL is performed, or modify the reward function parameterization. Recent work proposes a variational Bayes framework, Approximate Variational Reward Imitation Learning (AVRIL) [13], to approximate the full posterior. This method improves upon existing work by avoiding re-estimating Q^* for every sampled reward function, allowing it to bypass some of the computational inefficiencies of Ramachandran and Amir [34]’s initial formulation. However, AVRIL still requires the use of a Q -value function, resulting in a misspecified optimization objective. One method avoids using a Q -value function entirely for the likelihood [29] and instead approximates it using real-time dynamic programming or action comparison. Other work proposes a feature-based reward function, which parameterizes the reward as a linear combination of a set of weights and a low-dimensional feature encoding of the state [2, 17]. This approach can be beneficial because the posterior inference is over a lower dimensional reward vector. More recent work builds on this approach and proposes a method that enables imitation learning in complex control problems [9]. All of these techniques are best suited for environments with a closed-loop controller that provides instant feedback.

3 Methods

3.1 Conditional kernel density estimation

As discussed earlier, directly estimating the likelihood function can lead to theoretical guarantees of posterior consistency. To estimate the likelihood $p(s, a | R)$, we first observe that it can be viewed as the conditional density of the state-action pair given the reward function. Thus, any appropriate conditional density estimator could be applied; examples include the conditional kernel density estimator (CKDE, [44]) and Gaussian processes (GPs). We adopt the CKDE because it is nonparametric, has a closed form, and is straightforward to implement [19, 20]. Motivated by the conditional probability equation $p(y|x) = \frac{p(x,y)}{p(x)}$ (where x and y are two generic random variables), the CKDE estimates the conditional density $p(y|x)$ by approximating the joint distribution $p(x, y)$ and marginal distribution $p(x)$ separately via kernel density estimation (KDE). Given pairs of observations $\{(x_j, y_j)\}_{j=1}^m$, the KDE approximations for the joint and marginal distributions are

$$\hat{p}(x, y) = \frac{1}{m} \sum_{j=1}^m K\left(\frac{x - x_j}{h}\right) K'\left(\frac{y - y_j}{h'}\right), \quad \hat{p}(x) = \frac{1}{m} \sum_{j=1}^m K\left(\frac{x - x_j}{h}\right), \quad (3)$$

where K and K' are kernel functions with bandwidths $h, h' > 0$, respectively. To approximate the conditional density, the CKDE simply takes the ratio of these two KDE approximations:

$$\hat{p}(y|x) = \frac{\hat{p}(x, y)}{\hat{p}(x)} = \frac{\sum_{j=1}^m K\left(\frac{x-x_j}{h}\right) K'\left(\frac{y-y_j}{h'}\right)}{\sum_{\ell=1}^m K\left(\frac{x-x_\ell}{h}\right)}. \quad (4)$$

3.2 Kernel Density Bayesian IRL

We propose kernel density Bayesian inverse reinforcement learning (KD-BIRL), which uses a CKDE approximation $\hat{p}_m(s, a | R)$ to estimate the likelihood $p(s, a | R)$. While the standard form of the CKDE (Equation (4)) uses the difference between two samples (e.g., $x - x_j$) as input to the kernel functions, this difference can be replaced by any suitable distance metric [10]. To estimate the joint and marginal distributions, $p(s, a, R)$ and $p(R)$, we must specify two distance functions: one for comparing state-action tuples and one for comparing reward functions. We denote these as $d_s : (\mathcal{S} \times \mathcal{A}) \times (\mathcal{S} \times \mathcal{A}) \rightarrow \mathbb{R}_+$ and $d_r : \mathcal{R} \times \mathcal{R} \rightarrow \mathbb{R}_+$, respectively, and we discuss specific choices for them later. The CKDE approximation is then

$$\hat{p}_m(s, a | R) = \frac{\hat{p}_m(s, a, R)}{\hat{p}_m(R)} = \frac{\sum_{j=1}^m K\left(\frac{d_s((s, a), (s_j, a_j))}{h}\right) K'\left(\frac{d_r(R, R_j)}{h'}\right)}{\sum_{\ell=1}^m K\left(\frac{d_r(R, R_\ell)}{h'}\right)}, \quad (5)$$

where $h, h' > 0$ are the bandwidth hyperparameters.

Note that fitting a CKDE for the likelihood requires estimating the density across a range of reward functions and state-action pairs. To better enable this, we construct an additional set of demonstrations and reward functions – which we call the *training dataset* $\{(s_j, a_j, R_j)\}_{j=1}^m$ – to augment the observed expert demonstrations $\{(s_i^e, a_i^e)\}_{i=1}^n$ (from an agent acting according to the data generating reward R^*). The training dataset contains demonstrations from agents whose policies optimize for reward functions that are likely distinct from those of the expert. Each sample in the training dataset is a state-action pair associated with a reward function. There will be many state-action pairs that correspond to the same reward function; therefore, R_j is not unique. In a simulated setting where the training demonstrations are not available already, we choose k training set reward functions, learn k optimal policies that optimize for each of these functions, and generate $\lfloor m/k \rfloor$ demonstrations from each policy. We sample the reward functions $R_1, \dots, R_k \sim u$, where u is a distribution on the space of reward functions \mathcal{R} . The resulting density estimate is more accurate when R_1, \dots, R_k are uniformly distributed across \mathcal{R} . As such, in our experiments with simulated environments, we use a uniform distribution for u .

Using the CKDE in Equation (5), we can now estimate the posterior density function of R given n expert demonstrations, m training demonstrations, and prior $p(R)$:

$$\hat{p}_m^n(R | \{s_i^e, a_i^e\}_{i=1}^n) \propto p(R) \prod_{i=1}^n \hat{p}_m(s_i^e, a_i^e | R) = p(R) \prod_{i=1}^n \sum_{j=1}^m \frac{K\left(\frac{d_s((s_i^e, a_i^e), (s_j, a_j))}{h}\right) K'\left(\frac{d_r(R, R_j)}{h'}\right)}{\sum_{\ell=1}^m K\left(\frac{d_r(R, R_\ell)}{h'}\right)}. \quad (6)$$

The choice of the prior, $p(R)$, and the distance metrics d_s, d_r can be altered depending on information known about the reward function or state space in advance [3]. For example, if the reward function is assumed to be a linear function of the state, the cosine distance is more appropriate for d_r . Several non-uniform priors may be appropriate for $p(R)$ depending on the characteristics of the MDP, including Gaussian [32], Beta [34], and Chinese restaurant process (CRP) [27]. In KD-BIRL, the kernel $K(x) = \exp(-\|x\|^2)$ is chosen to be Gaussian. We choose a Gaussian kernel because it can approximate bounded and continuous functions well. The bandwidth hyperparameters can be chosen using rule-of-thumb procedures [41].

To infer the posterior estimate in Equation (6), we sample rewards using a Hamiltonian Monte Carlo algorithm [43] (additional details in Appendix Section 9). Note a key computational gain of our approach over BIRL, which is also a sampling-based algorithm: we only use forward RL to generate the training dataset (in the case of simulated environments or when it is not already present), and avoid it in each iteration of MCMC. This is possible because Equation (6) does not depend on Q^* .

3.2.1 Feature-based reward function

While KD-BIRL can be applied as-is in many environments, the CKDE is known to scale poorly to high-dimensional functions. Thus, before KD-BIRL can work in environments with large state spaces where the corresponding reward

function has a large number of parameters, it is necessary to re-parameterize the reward function. In our existing formulation, the reward function is parameterized as a vector where each index corresponds to the reward in one of the states. Under this formulation, in a 10×10 Gridworld environment, the reward function would be represented as a vector of length 100. In practice, the CKDE increases in computational cost with respect to both the length of the vector and the number of samples in the expert and training datasets [21], and it would not be suited to learn 100 parameters.

We propose a formulation of KD-BIRL that uses a *feature-based reward function* [35]. This method of parameterizing a reward is one of three broad categories of IRL formulations [1]. The feature-based reward function $R(s, a) = w^\top \phi(s, a)$ where $w \in \mathcal{R}^q$ and $\phi : S \times A \rightarrow \mathcal{R}^q$ is advantageous because it does not scale with the dimensionality of the state s and does not rely on the state space being discrete like our earlier approach. Here, ϕ is a known function that maps a state-action tuple to a feature vector of length q . Intuitively, this feature vector is a low-dimensional representation of the original state that facilitates reward inference. In this setup, the goal is to find w^* such that:

$$w^{*\top} E \left[\sum_{t=0}^{\infty} \gamma^t \phi(s_t, a_t) | \pi^* \right] \geq w^{*\top} E \left[\sum_{t=0}^{\infty} \gamma^t \phi(s_t, a_t) | \pi \right]$$

where γ is a discount factor, π is a policy, and s_t, a_t is the state and action at time t . In a Bayesian setting, the resulting posterior is over w rather than R .

Now we generate n expert and m training demonstrations. Recall that the CKDE requires as input the reward function parameters corresponding to each training dataset sample. A given training dataset sample here is $\{(s_j, a_j, w_j)\}$ where w_j is the weight vector of length q associated with the reward function that was used by the agent to generate the sample s_j, a_j . w_j can be repeated and is not unique. A sample from the expert demonstration dataset is still $\{(s_i^e, a_i^e)\}_{i=1}^n$, where the data-generating weights w^* are used to generate these demonstrations. The procedure for learning the CKDE and the resulting posterior inference then stays the same. The CKDE formulation is now:

$$\hat{p}_m(s, a | w) = \frac{\hat{p}_m(s, a, w)}{\hat{p}_m(w)} = \sum_{j=1}^m \frac{K\left(\frac{d_s((s, a), (s_j, a_j))}{h}\right) K'\left(\frac{d_r(w, w_j)}{h'}\right)}{\sum_{\ell=1}^m K\left(\frac{d_r(w, w_\ell)}{h'}\right)}, \quad (7)$$

where d_r measures the similarity between weight vectors, and d_s is the distance between state-action tuples. The posterior is then:

$$\hat{p}_m^n(w | \{s_i^e, a_i^e\}_{i=1}^n) \propto p(w) \prod_{i=1}^n \hat{p}_m(s_i^e, a_i^e | w) = p(w) \prod_{i=1}^n \sum_{j=1}^m \frac{K\left(\frac{d_s((s_i^e, a_i^e), (s_j, a_j))}{h}\right) K'\left(\frac{d_r(w, w_j)}{h'}\right)}{\sum_{\ell=1}^m K\left(\frac{d_r(w, w_\ell)}{h'}\right)}. \quad (8)$$

4 Theoretical guarantees of KD-BIRL

KD-BIRL estimates the density function of a true Bayesian posterior distribution (Equation (6)), so we can reason about the posterior’s asymptotic behavior. In particular, we want to ascertain that this posterior estimate contracts as it receives more samples. Because the IRL problem is non-identifiable, the “correct” reward function as defined by existing methods [2, 36, 49, 50], may not be unique. In this work, we assume that any two reward functions that lead an agent to behave in the same way are equivalent. Said another way, if a set of observations is equally likely under two reward functions, the functions are considered equal: $R_1 \simeq R_2$ if $\|p(\cdot | R_1) - p(\cdot | R_2)\|_{L_1} = 0$. We can then define the *equivalence class* $[R^*]$ for R^* as $[R^*] = \{R \in \mathcal{R} : R \simeq R^*\}$. An ideal posterior distribution places higher mass on reward functions in the equivalence class $[R^*]$.

We first focus on the likelihood estimation step of our approach and show that, when the size of the training dataset m approaches ∞ and the m samples arise from sufficiently different reward functions that cover the space of \mathcal{R} , the likelihood estimated using a CKDE (Equation (5)) converges to the true likelihood $p(s, a | R)$.

Lemma 4.1. *Let $h_m, h'_m > 0$ be the bandwidths chosen for the CKDE. Assume that both $p(s, a | R)$ and $p(R)$ are square-integrable and twice differentiable with a square-integrable and continuous second order derivative, and that $mh_m^{p/2} \rightarrow \infty$ and $mh'_m{}^{p/2} \rightarrow \infty$ as $m \rightarrow \infty$. Then,*

$$\hat{p}_m(s, a | R) \xrightarrow[m \rightarrow \infty]{P} p(s, a | R), \quad \forall (s, a, R) \in \mathcal{S} \times \mathcal{A} \times \mathcal{R}.$$

Lemma 4.1 verifies that we can estimate the likelihood using a CKDE, opening the door to Bayesian inference. We now show that as n , the size of expert demonstrations, and m , the size of the training dataset, approach ∞ , the posterior distribution generated using KD-BIRL contracts to the equivalence class of the expert demonstration generating reward $[R^*]$.

Theorem 4.2. Assume the prior for R , denoted by Π , satisfies $\Pi(\{R : \text{KL}(R^*, R) < \epsilon\}) > 0$ for any $\epsilon > 0$, where KL is the Kullback–Leibler divergence. Assume $\mathcal{R} \subseteq \mathbb{R}^d$ is a compact set. Then, the posterior measure corresponding to the posterior density function \hat{p}_m^n defined in Equation (6), denoted by Π_m^n , is consistent w.r.t. the L_1 distance; that is,

$$\Pi_m^n(\{R : \|p(\cdot|R) - p(\cdot|R^*)\|_{L_1} < \epsilon\}) \xrightarrow[n \rightarrow \infty]{m \rightarrow \infty} 1.$$

Theorem 4.2 implies that the posterior Π_m^n assigns almost all mass to the neighborhood of $[R^*]$. This means that the reward function the KD-BIRL posterior contracts to with a large enough sample size is practically equivalent to the data-generating reward function R^* . Note that this is not a statement regarding the posterior contraction rate, just a certification of contraction. Proofs for both Theorem 4.2 and Lemma 4.1 are in Appendix Section 4.

5 Experiments

Here, we evaluate the accuracy and computational efficiency of KD-BIRL. We compare KD-BIRL to AVRIL [13], a recent method that simultaneously learns an imitator policy and performs reward inference on the expert demonstrations, and the original Bayesian IRL algorithm (BIRL) [34]. We demonstrate results using a Gridworld environment [7] and a sepsis management clinical environment [4].

To quantitatively evaluate the reward functions learned by IRL methods, previous studies have used Expected Value Difference (EVD) [8, 14, 15, 25]. EVD is defined as $|V^*(r^A) - V^{\pi^*(r^L)}(r^A)|$ where $V^\pi = \sum_s p_0(s) V^\pi$ is the value of policy π with initial state distribution p_0 , r^A is the true data-generating reward, r^L is the learned reward, and V^* is the value function associated with the optimal policy π^* . Intuitively, the EVD measures the difference in reward obtained by an agent whose policy is optimal for the true reward and the reward obtained by an agent whose policy is optimal for the learned reward. We use EVD because it allows us to compare KD-BIRL to related methods without needing to directly compare two reward function samples based on their functional form. The lower the EVD, the better our learned reward recapitulates the expert reward (see Appendix Section 10 for more details).

5.1 Gridworld environment

We begin our analysis in a Gridworld environment. The MDP here is defined by the grid’s $g \times g$ discrete state space \mathcal{S} where a given state is represented as a one-hot encoded vector in $\mathcal{R}^{g \times g}$, e_i , where the i ’th index is 1 and corresponds to the state in which the agent is in, and g is the size of the grid; the action space contains 5 possible actions $\{\text{NO ACTION}, \text{UP}, \text{RIGHT}, \text{LEFT}, \text{DOWN}\}$, each represented as a one-hot encoded vector; and the true reward function R^* , which is unobserved by the IRL algorithms, is a vector of length $g \times g$. We structure the reward function such that each state has an independent scalar reward parameter. We specify the domain of each of these parameters to be the unit interval; thus, each feasible reward function can be represented by a vector $R \in [0, 1]^{g \times g}$.

To fit KD-BIRL we use Stan [43], which uses a Hamiltonian Monte Carlo algorithm. To fit the BIRL and AVRIL posteriors, we first generate the same number of expert demonstration trajectories as used for KD-BIRL. BIRL and AVRIL use an inverse temperature hyperparameter, α ; we set $\alpha = 1$ for all methods. AVRIL uses two additional hyperparameters γ, δ , which we set to 1. Unless otherwise specified, KD-BIRL uses a uniform prior for the reward $r_s \sim \text{Unif}(0, 1)$ for $s = 1, \dots, g \times g$ and Euclidean distance for d_s, d_r .

5.1.1 Visualizing KD-BIRL’s posterior distribution

First, we visualize KD-BIRL’s posterior distribution in comparison to those recovered by AVRIL and BIRL. To do this, we show density plots of samples from all three distributions marginalized at each state in the 2×2 Gridworld environment. All methods use a data-generating reward function $R^* = [0, 0, 0, 1]$. We find that the posterior samples from KD-BIRL and BIRL are more concentrated around R^* than those from AVRIL (Figure 1).

5.1.2 KD-BIRL requires fewer instances of Q-learning

Next, we quantify the computational complexity associated with performing reward inference in a 4×4 Gridworld in which only the state $[3, 3]$ contains a reward of 1. As discussed earlier, much of the computational cost associated with learning a posterior distribution in existing methods arises from repeated instances of forward RL. BIRL requires forward RL during every iteration of MCMC sampling; several thousand iterations are required for the sampler to converge. AVRIL uses one instance of forward RL to learn an approximate posterior. KD-BIRL also minimizes the use of forward RL, only using it during dataset generation, in the case that these observations are not already available.

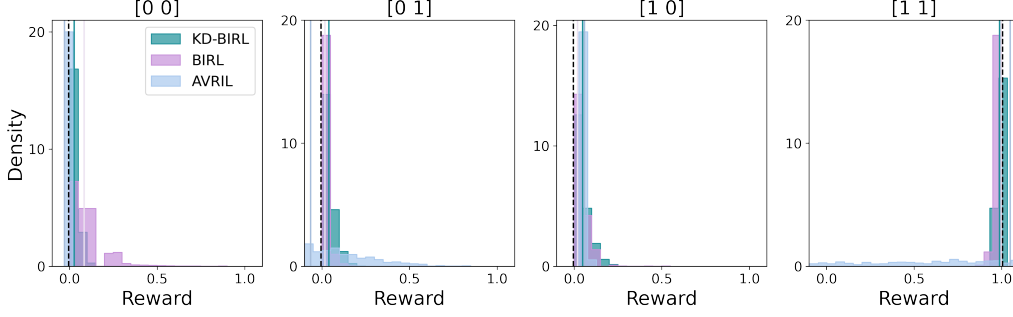


Figure 1: **Marginalized posterior distribution in a 2×2 Gridworld** where the data generating reward function $R^* = [0, 0, 0, 1]$. The dashed vertical lines display the true reward in each state. Each algorithm’s mean estimated reward is shown using vertical colored lines. The x-axis corresponds to the numeric value of the sampled reward marginalized by the given state. KD-BIRL’s and BIRL’s marginal posterior distributions are more concentrated around the true reward R^* compared to those of AVRIL.

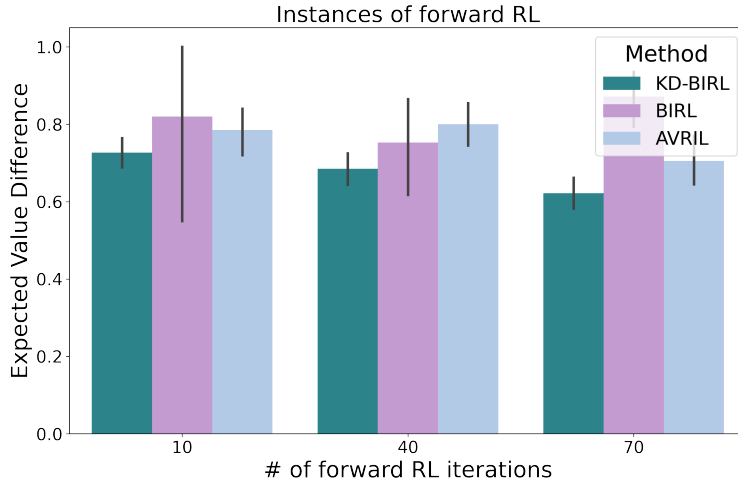


Figure 2: **KD-BIRL requires fewer instances of forward RL to generate samples with lower EVD** in a 4×4 Gridworld where only the state $[3, 3]$ receives a reward of 1.0. The BIRL reward samples continue to have high EVDs even with many instances of RL (each corresponding to an iteration of MCMC), and AVRIL only performs RL once, but the resulting EVDs stagnate.

Here, we vary the number of iterations of forward RL and plot the EVDs for reward samples from the resulting posterior distributions for the three methods. Our results indicate that with fewer instances of forward RL, KD-BIRL reward samples better replicate the behavior of the expert demonstrations than those of BIRL (partly because the x-axis implies too few iterations of MCMC sampling); consequently, even though AVRIL requires fewer instances of forward RL, it is at the expense of accuracy in the posterior distribution, as highlighted by the stagnant EVD (Figure 2).

5.2 Limitations of the CKDE

It is well known that CKDE has difficulty scaling to high-dimensional probability density functions [21]. Regardless, we want to identify the limits of the CKDE used in the original KD-BIRL setup without a feature-based reward function. To do so, we use a 5×5 Gridworld environment. In Figure 3, despite the fact that the number of reward parameters is larger than what we expect the CKDE to successfully model, KD-BIRL is able to estimate a posterior whose mean is in the equivalence class of R^* . That is, the posterior mean and R^* encourage the same behavior in an agent, which implies that the expert demonstrations are equally likely under both. However, there are states $([2, 3], [4, 3])$ in Figure 3, Panel 2) in the 5×5 Gridworld in which the mean estimated reward is notably incorrect, which indicates that the CKDE struggles to learn 25 independent reward parameters successfully.

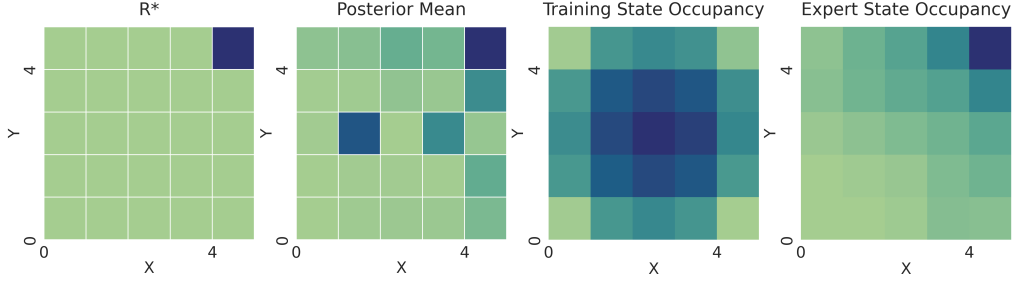


Figure 3: **Pushing the CKDE’s limits in a 5×5 Gridworld environment.** The first panel shows R^* , the second panel shows the KD-BIRL posterior mean, and the third and fourth panels show the training and expert demonstrations state occupancy respectively. The KD-BIRL posterior mean is within the equivalence class of R^* , because the darkest square is in the upper right hand corner, even though there are some dark squares in other portions of the grid.

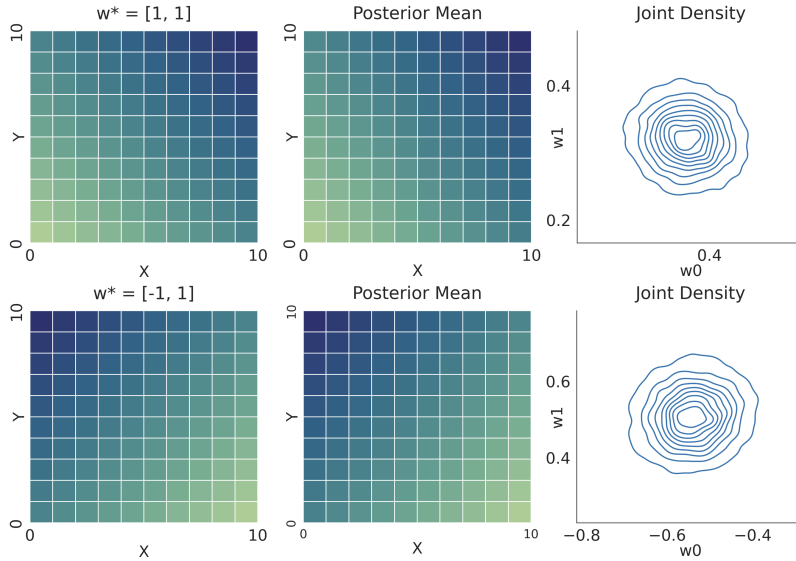


Figure 4: **Feature-based reward in a 10×10 Gridworld** for $w^* = [1, 1]$ (top) and $w^* = [-1, 1]$ (bottom). The first images in each row visualize w^* projected onto the Gridworld, the second visualize the mean of the KD-BIRL posterior projected onto the Gridworld, and the third images show the joint density plots of the two weights, with the first on the x-axis and the second on the y-axis. KD-BIRL accurately infers the relative magnitude and sign of the individual weights.

5.3 Feature-based rewards

We now study three methods of reward function featurization that can enable KD-BIRL to perform reward inference in environments with large state spaces.

5.3.1 Using known features in a 10x10 Gridworld

As discussed in Section 3.2.1, without using feature-based rewards, the original KD-BIRL algorithm would not be able to perform inference in the 10×10 Gridworld because the reward vector length (100) is too high. In the 10×10 Gridworld, the MDP is identical to the earlier Gridworld settings, except the state space is the series of one-hot encoded vectors of length 100. In this setting, we select $\phi(s) = [x, y]$ to be a simple function that ignores the action and maps the state vector of length 100 to the spatial coordinates of the agent. In this way, we treat the coordinates of the agent as a “feature vector”. Then, we choose weights w^* such that R^* is a linear combination of the features and w^* . Figure 4 visualizes the resulting posterior distributions for two choices of w^* . We use a Normal prior for $p(w)$ with mean 0 and variance 1 for $w^* = [-1, 1]$, and a Normal prior with mean 0.5 and variance 0.5 for $w^* = [1, 1]$. We find that KD-BIRL accurately recovers the relative magnitude and sign of the individual components of w^* for both chosen reward functions.

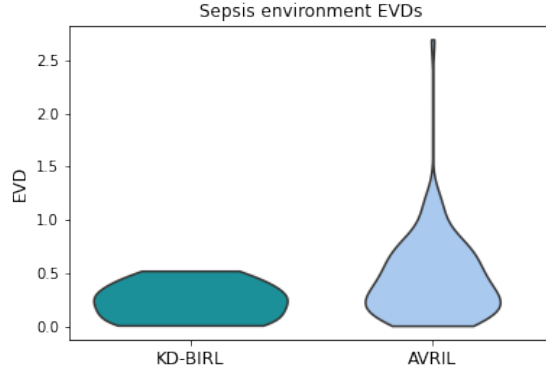


Figure 5: **Evaluating manually curated feature-based reward in the sepsis environment.** We plot the EVD for 100 reward samples from KD-BIRL and 100 trajectories from AVRIL. KD-BIRL’s EVDs are more concentrated around 0 than those of AVRIL, indicating that the reward samples from KD-BIRL’s posterior better replicate the demonstrations from the data-generating reward.

5.3.2 Manually curated features in a sepsis treatment environment

Now we perform inference in a sepsis treatment simulator based on de-identified data from MIMIC-III [16, 22], a database of electronic health records (EHR). Sepsis arises when the body responds to infection in a way that is harmful to its own tissues and organs [11]. In the original simulator [4], the state is a vector of length 46, where each element contains information about a given physiological covariate. There are 25 possible actions, each corresponding to a different combination of treatments. The transition function was learned using deep RL models [33] (see Appendix Section 12 for details).

Sepsis treatment depends heavily on organ failure metrics, and fast increases in these metrics warrant urgent care [33]. Since we have observed that in the Gridworld environment, KD-BIRL can successfully model a reward that is a function of a small state space, we choose ϕ to be a function that ignores the action and extracts three Sequential Organ Failure Assessment (SOFA) [23] covariates present in the state: *sofa*, *quick sofa*, and *quick sofa systolic blood pressure score*. The result is a feature-based reward function with manually selected features based on prior knowledge. Our reward is now a linear combination of the difference between the state features at time t and $t + 1$,

$$R(s_t) = \begin{bmatrix} a \\ b \\ c \end{bmatrix}^\top \begin{bmatrix} s(\text{cov}_1)_t - s(\text{cov}_1)_{t+1} \\ s(\text{cov}_2)_t - s(\text{cov}_2)_{t+1} \\ s(\text{cov}_3)_t - s(\text{cov}_3)_{t+1} \end{bmatrix}$$

where $[a, b, c]$ are the weights, and $s(\text{cov}_1)$, $s(\text{cov}_2)$, $s(\text{cov}_3)$ are the three organ failure features in state s . We choose the true (unobserved) weights to be $[a = 0.8, b = 0.6, c = 0.4]$. We compare our method to AVRIL and avoid fitting BIRL due to computational constraints. Our results indicate that KD-BIRL generates reward samples with lower and more concentrated EVDs than the AVRIL trajectories (Figure 5). This indicates that KD-BIRL estimates a posterior distribution that is concentrated around the equivalence class of R^* .

5.3.3 Using a VAE to identify features in the sepsis environment

Finally, we explore the use of a variational auto-encoder (VAE) to learn ϕ in the sepsis environment. More specifically, we use a VAE to learn a low-dimensional representation of state-action tuples, and aim to learn the set of weights that modifies this representation to form the reward function. To do this, we first learn ϕ on a set of state-action tuples independent of the *training* or *expert* demonstrations. The input dimension to the VAE is 47 (46 state features + 1 action), and the low dimensional representation has 3 features. The VAE uses 4 linear layers for the encoder and decoder, and optimizes for a downsampled representation with low reconstruction error using Adam.

Once ϕ is known, it can be used to generate the required datasets. To do this, we first select a set of weights w^* for the expert demonstrations, and generate state-action tuples that optimize $R(s, a)$ where $R(s, a) = \phi(s, a) \times w^*$. We repeat this procedure for several sets of uniformly selected weights w_0, \dots, w_c to generate the training dataset. Finally, we fit KD-BIRL and evaluate the learned weights using EVD as before. We report results in Table 1, and find that across a variety of w^* values, KD-BIRL’s posterior samples generate comparable, if not much lower values than AVRIL. This, coupled with the additional theoretical guarantees, makes KD-BIRL a good choice for performing IRL in complex environments.

Table 1: **Evaluating using a VAE for ϕ in the sepsis environment.** We report mean \pm standard deviation of EVD across 50 posterior samples (KD-BIRL) and 50 trajectories (AVRIL).

w^*	EVD	
	KD-BIRL	AVRIL
[0.1, 0.2, 0.3]	5.51 \pm 1.55	5.64 \pm 1.2
[0.3, 0.2, 0.5]	8.58 \pm 2.3	9.41 \pm 2.23
[0.5, 0.5, 0.5]	14.45 \pm 3.09	13.25 \pm 3.25
[0.6, 0.8, 1.0]	21.95 \pm 4.85	27.55 \pm 6.49
[0.8, 0.6, 0.4]	19.15 \pm 7.58	19.41 \pm 8.3

6 Discussion and Conclusion

In this work, we present kernel density Bayesian inverse reinforcement learning (KD-BIRL), an efficient IRL algorithm that improves upon existing methods by estimating a posterior distribution on the reward function while avoiding Q -learning for every iteration of MCMC sampling, and by providing theoretical guarantees of posterior consistency. We show that KD-BIRL generates concentrated posteriors and is more computationally efficient than existing methods in a Gridworld environment. Additionally, we demonstrate that with a feature-based reward function, KD-BIRL can perform inference in a complex healthcare environment, and the resulting posterior outperforms a leading method. Taken together, our results suggest that, in complex environments, KD-BIRL can enable an accurate probabilistic description of clinician objectives that is not possible with current methods.

Several future directions remain. This work is best-suited for on-policy (i.e., simulation) environments, and additional work is necessary to apply it directly to off-policy environments such as retrospective clinical decision-making settings. In particular, we would need behavior demonstrations from multiple agents in order to define a training dataset. Thus, it will be necessary to be able to associate actions with an agent (i.e., clinician). Additionally, the particular choices of distance metrics and hyperparameters used in the CKDE depend on the environment and reward function parameterization; additional experimentation is required to adapt this to different environments. Furthermore, a limitation of the conventional CKDE is that it performs poorly in high dimensions. One solution is to consider a modified version of the CKDE to speed it up [19]. Another solution is to replace the CKDE with another nonparametric conditional density estimator [18, 37]. Because KD-BIRL is a framework that estimates the likelihood as a conditional density, it can be easily modified to accommodate other choices for the CKDE. Finally, in this work, we discuss efforts to re-parameterize the reward function, and it is of interest to apply this work in additional environments with continuous or infinite state spaces, such as real-world EHR.

Acknowledgments and Disclosure of Funding

We thank Alex Chan for providing code associated with the AVRIL method. This work was funded by the Helmsley Trust grant AWD1006624, NIH NCI 5U2CCA233195, NIH NHLBI R01 HL133218, and NSF CAREER AWD1005627. BEE is on the SAB of Creyon Bio, Arrepath, and Freenome. A. Mandyam was supported in part by a Stanford Engineering Fellowship. D. Cai was supported in part by a Google Ph.D. Fellowship in Machine Learning.

References

- [1] Pieter Abbeel. Inverse reinforcement learning. URL <https://people.eecs.berkeley.edu/~pabbeel/cs287-fa12/slides/inverseRL.pdf>.
- [2] Pieter Abbeel and Andrew Y. Ng. Apprenticeship learning via inverse reinforcement learning. In *The Twenty-First International Conference on Machine Learning*, 2004.
- [3] Stephen Adams, Tyler Cody, and Peter A. Beling. A survey of inverse reinforcement learning. *Artificial Intelligence Review*, Feb 2022.
- [4] Peter Henderson Amirhossein Kiani, Tianli Ding. Gymic: An OpenAI gym environment for simulating Sepsis treatment for ICU patients. <https://github.com/akiani/rlsepsis234>, 2019.
- [5] Sreejith Balakrishnan, Quoc Phong Nguyen, Bryan Kian Hsiang Low, and Harold Soh. Efficient exploration of reward functions in inverse reinforcement learning via Bayesian optimization. *arXiv preprint arXiv:2011.08541*, 2020.

- [6] P. G. Bissiri, C. C. Holmes, and S. G. Walker. A general framework for updating belief distributions. *Journal of the Royal Statistical Society. Series B (Statistical Methodology)*, 78(5), 2016.
- [7] Greg Brockman, Vicki Cheung, Ludwig Pettersson, Jonas Schneider, John Schulman, Jie Tang, and Wojciech Zaremba. OpenAI gym. *arXiv preprint arXiv:1606.01540*, 2016.
- [8] Daniel S. Brown and Scott Niekum. Efficient probabilistic performance bounds for inverse reinforcement learning. In *AAAI*, 2018.
- [9] Daniel S. Brown, Russell Coleman, Ravi Srinivasan, and Scott Niekum. Safe imitation learning via fast Bayesian reward inference from preferences. *CoRR*, abs/2002.09089, 2020.
- [10] Gavin C. Cawley and Nicola L. C. Talbot. On over-fitting in model selection and subsequent selection bias in performance evaluation. *Journal of Machine Learning Research*, 11(70):2079–2107, 2010.
- [11] CDC. Sepsis is a medical emergency. Act fast., Apr 2022. URL <https://www.cdc.gov/sepsis/what-is-sepsis.html>.
- [12] J.E. Chacón and T. Duong. *Multivariate Kernel Smoothing and Its Applications*. Chapman and Hall/CRC Monographs on Statistics and Applied Probability Series. CRC Press, Taylor & Francis Group, 2018. ISBN 9781498763011. URL <https://books.google.com/books?id=ur6-tAEACAAJ>.
- [13] Alex James Chan and Mihaela van der Schaar. Scalable Bayesian inverse reinforcement learning. In *International Conference on Learning Representations*, 2021.
- [14] Jaedeug Choi and Kee-eung Kim. Nonparametric Bayesian inverse reinforcement learning for multiple reward functions. In *Advances in Neural Information Processing Systems*, 2012.
- [15] Jaedeug Choi and Kee-Eung Kim. Bayesian nonparametric feature construction for inverse reinforcement learning. In *The Twenty-Third International Joint Conference on Artificial Intelligence*, 2013.
- [16] Ary L Goldberger, Luis AN Amaral, Leon Glass, Jeffrey M Hausdorff, Plamen Ch Ivanov, Roger G Mark, Joseph E Mietus, George B Moody, Chung-Kang Peng, and H Eugene Stanley. Physiobank, Physiokit, and Physionet: components of a new research resource for complex physiologic signals. *Circulation*, 2000.
- [17] Dylan Hadfield-Menell, Smitha Milli, Pieter Abbeel, Stuart Russell, and Anca Dragan. Inverse reward design. 2017. URL <https://arxiv.org/abs/1711.02827>.
- [18] Fabian Hinder, Valerie Vaquet, Johannes Brinkrolf, and Barbara Hammer. Fast non-parametric conditional density estimation using moment trees. In *2021 IEEE Symposium Series on Computational Intelligence (SSCI)*, pages 1–7. IEEE, 2021.
- [19] Michael P. Holmes, Alexander G. Gray, and Charles Lee Isbell. Fast nonparametric conditional density estimation. In *The Twenty-Third Conference on Uncertainty in Artificial Intelligence*, UAI, 2007.
- [20] Rafael Izbicki and Ann B. Lee. Nonparametric conditional density estimation in a high-dimensional regression setting. *Journal of Computational and Graphical Statistics*, 25(4):1297–1316, 2016.
- [21] Rafael Izbicki and Ann B. Lee. Converting high-dimensional regression to high-dimensional conditional density estimation. 2017. URL <https://arxiv.org/abs/1704.08095>.
- [22] Alistair EW Johnson, Tom J Pollard, Lu Shen, H Lehman Li-Wei, Mengling Feng, Mohammad Ghassemi, Benjamin Moody, Peter Szolovits, Leo Anthony Celi, and Roger G Mark. MIMIC-III, a freely accessible critical care database. *Scientific data*, 3(1):1–9, 2016.
- [23] Alan E. Jones, Stephen Trzeciak, and Jeffrey A. Kline. The sequential organ failure assessment score for predicting outcome in patients with severe sepsis and evidence of hypoperfusion at the time of emergency department presentation. *Critical care medicine*, 37(5):1649–1654, May 2009.
- [24] J Zico Kolter, Pieter Abbeel, and Andrew Y Ng. Hierarchical apprenticeship learning with application to quadruped locomotion. In *Advances in Neural Information Processing Systems*, pages 769–776. Citeseer, 2008.
- [25] Sergey Levine, Zoran Popović, and Vladlen Koltun. Nonlinear inverse reinforcement learning with Gaussian processes. In *The 24th International Conference on Neural Information Processing Systems*, NIPS, page 19–27, 2011.
- [26] Henry B Mann and Abraham Wald. On stochastic limit and order relationships. *The Annals of Mathematical Statistics*, 14(3):217–226, 1943.
- [27] Bernard Michini and Jonathan P. How. Bayesian nonparametric inverse reinforcement learning. In *Machine Learning and Knowledge Discovery in Databases*, pages 148–163, 2012.
- [28] Bernard Michini and Jonathan P. How. Improving the efficiency of Bayesian inverse reinforcement learning. In *2012 IEEE International Conference on Robotics and Automation*, pages 3651–3656, May 2012.

- [29] Bernard Michini, Mark Cutler, and Jonathan P. How. Scalable reward learning from demonstration. In *2013 IEEE International Conference on Robotics and Automation*, pages 303–308, 2013.
- [30] Katja Mombaur, Anh Truong, and Jean-Paul Laumond. From human to humanoid locomotion—an inverse optimal control approach. *Autonomous Robots*, 28(3):369–383, 2010.
- [31] Andrew Y. Ng and Stuart Russell. Algorithms for inverse reinforcement learning. In *Proc. 17th International Conf. on Machine Learning*, pages 663–670, 2000.
- [32] Qifeng Qiao and Peter A. Beling. Inverse reinforcement learning with Gaussian process. *2011 American Control Conference*, pages 113–118, 2011.
- [33] Aniruddh Raghu, Matthieu Komorowski, Leo Anthony Celi, Peter Szolovits, and Marzyeh Ghassemi. Continuous state-space models for optimal Sepsis treatment: a deep reinforcement learning approach. In *MLHC*, 2017.
- [34] Deepak Ramachandran and Eyal Amir. Bayesian inverse reinforcement learning. In *The 20th International Joint Conference on Artificial Intelligence*, page 2586–2591, 2007.
- [35] Nathan Ratliff, David Bradley, J. Andrew Bagnell, and Joel Chestnutt. Boosting structured prediction for imitation learning. In *Advances in Neural Information Processing Systems*, page 1153–1160, 2006.
- [36] Nathan D. Ratliff, J. Andrew Bagnell, and Martin A. Zinkevich. Maximum margin planning. In *The 23rd International Conference on Machine Learning, ICML*, page 729–736, 2006.
- [37] Alex L Rojas, Christopher R Genovese, Christopher J Miller, Robert Nichol, and Larry Wasserman. Conditional density estimation using finite mixture models with an application to astrophysics. *Center for Automatic Learning and Discovery, Department of Statistics, Carnegie Mellon University*, 2005.
- [38] Constantin A. Rothkopf and Dana H. Ballard. Modular inverse reinforcement learning for visuomotor behavior. *Biol. Cybern.*, 107(4):477–490, aug 2013. ISSN 0340-1200.
- [39] Lorraine Schwartz. On Bayes procedures. *Zeitschrift für Wahrscheinlichkeitstheorie und Verwandte Gebiete*, 4: 10–26, 1965.
- [40] John Shawe-Taylor and Robert C Williamson. A PAC analysis of a Bayesian estimator. In *The tenth annual conference on Computational learning theory*, pages 2–9, 1997.
- [41] B. W. Silverman. *Density Estimation for Statistics and Data Analysis*. Chapman & Hall, London, 1986.
- [42] Richard S. Sutton and Andrew G. Barto. *Reinforcement Learning: An Introduction*. A Bradford Book, Cambridge, MA, USA, 2018. ISBN 0262039249.
- [43] Stan Development Team. Stan modeling language users guide and reference manual, version 2.29, 2011. URL <https://mc-stan.org/>.
- [44] Aad van der Vaart. *Asymptotic Statistics*, volume 3. Cambridge University Press, 2000.
- [45] Adrian Šošić, Abdelhak M. Zoubir, Elmar Rueckert, Jan Peters, and Heinz Koepl. Inverse reinforcement learning via nonparametric spatio-temporal subgoal modeling. *J. Mach. Learn. Res.*, 19(1):2777–2821, jan 2018. ISSN 1532-4435.
- [46] Matt P Wand and M Chris Jones. *Kernel smoothing*. CRC press, 1994.
- [47] Tong Zhang. From epsilon-entropy to KL-entropy: Analysis of minimum information complexity density estimation. *The Annals of Statistics*, 34(5), oct 2006.
- [48] Jiangchuan Zheng, Siyuan Liu, and Lionel M. Ni. Robust Bayesian inverse reinforcement learning with sparse behavior noise. In *Association for the Advancement of Artificial Intelligence, AAAI’14*, page 2198–2205, 2014.
- [49] Brian D Ziebart, Andrew L Maas, J Andrew Bagnell, Anind K Dey, et al. Maximum entropy inverse reinforcement learning. In *Association for the Advancement of Artificial Intelligence (AAAI)*, volume 8, pages 1433–1438, 2008.
- [50] Brian D. Ziebart, Andrew L. Maas, J. Andrew Bagnell, and Anind K. Dey. Human behavior modeling with maximum entropy inverse optimal control. In *AAAI Spring Symposium: Human Behavior Modeling*, 2009.

A Code

Our experiments were run on an internally-hosted cluster using a 320 NVIDIA P100 GPU whose processor core has 16 GB of memory hosted. Our experiments used a total of approximately 200 hours of compute time. Our code uses the MIT License and is available at <https://github.com/bee-hive/kdbirl>.

B Rationality of Bayesian IRL

The original Bayesian IRL algorithm uses a Q -value function as a component of the likelihood calculation. While this can be sufficient for imitation learning, it does not allow for posterior predictive sampling, and updates to the Gibbs posterior are not rational unless the Q -value function satisfies certain conditions [6] (see Appendix C). Intuitively, rational updates imply that new evidence is appropriately incorporated to modify the posterior from the prior. The Q -value function can be approximated using any real-value prediction method from neural networks to linear regression, and the rationality of the resulting posterior updates is not discussed in prior work. A rational posterior update implies that if the updating function, in this case, Q^* , has a lower value, the posterior probabilities should be lower, and vice versa. However, there is no way to confirm that Q^* satisfies Assumption 3 of the guidelines for updating belief distributions in Bissiri et al. [6]. Furthermore, a Q -value function is a poor approximation of density or likelihood. A higher Q -value associated with a state means that the Q -learning algorithm finds that this state is more likely to generate a reward. However, this does not imply that an agent is more likely to visit that state. Bayesian IRL formulations that use a Q -value function equate these two phenomena, and this can be incorrect depending on (1) the optimality of such an agent, (2) the quality of the Q -learning estimator, and (3) whether the agent has even visited the state.

C Rationality conditions for posterior distribution updates

Bissiri et al. [6] make several assumptions before guaranteeing rational updates to a posterior distribution. These are:

Assumption 1.

$$\psi[l(\theta, x_2), \psi\{l(\theta, x_1), \pi(\theta)\}] \equiv \psi\{l(\theta, x_1) + l(\theta, x_2), \pi(\theta)\}$$

where θ is the parameter of interest, $\pi(\theta)$ is the prior distribution on θ , l is a loss function, ψ is the update function, and x_1, x_2 are data points.

Assumption 2. For any set $A \subset \Theta$,

$$\frac{\psi\{l(\theta, x), \pi(\theta)\}}{\int_A \psi\{l(\theta, x), \pi(\theta)\} d\theta} = \psi\{l(\theta, x), \pi_A(\theta)\}$$

where π_A is π normalized to A .

Assumption 3. Lower evidence for a state should yield smaller posterior probabilities under the same prior. So, if for some $A \subset \Theta$, $l(\theta, x) > l(\theta, y)$ for $\theta \in A \subset \Theta$ and $l(\theta, x) = l(\theta, y)$ for $\theta \in A^c$, then

$$\int_A \psi\{l(\theta, x), \pi(\theta)\} d\theta < \int_A \psi\{l(\theta, y), \pi(\theta)\} d\theta.$$

Assumption 4. If $l(\theta, x) \equiv \text{constant}$, then $\psi\{l(\theta, x), \pi(\theta)\} \equiv \pi(\theta)$.

Assumption 5. If $\tilde{l}(\theta, x) = l(\theta, x) + c$ for some constant c , then

$$\psi\{\tilde{l}(\theta, x), \pi(\theta)\} = \psi\{l(\theta, x), \pi(\theta)\}.$$

If ψ is a Q -value function, which can be parameterized by anything from a linear model to a deep neural network, the rationality of the subsequent posterior updates is not discussed in previous work. In particular, it is not possible to verify these assumptions for a Q -value function.

D Proofs for Lemma 4.1, Theorem 4.2

The proof associated with Lemma 4.1 follows.

Proof. We now use the continuity of the likelihood, the finite sample analysis of multivariate kernel density estimators in Wand and Jones [46][Section 4.4, Equation 4.16](Appendix F), which defines the Mean Integrated Square Error

(MISE) of the density function, and Theorem 1 (Appendix E) of Chacón and Duong [12][Section 2.6-2.9], which asserts that as the sample size increases, the mean of the density estimator converges and variance prevents the mean from exploding. We can use Theorem 1 because we assume that the density function is square-integrable and twice differentiable and that the bandwidth approaches 0 as the dataset size increases. Then, up to a constant, for a given state-action pair (s, a) ,

$$\frac{1}{m} \sum_{j=1}^m e^{-d_s((s,a),(s_j,a_j))^2/(2h)} e^{-d_r(R,R_j)^2/(2h')} \xrightarrow[m \rightarrow \infty]{P} p(s, a, R).$$

The same holds true for d_r , $\frac{1}{m} \sum_{\ell=1}^m e^{-d_r(R,R_\ell)^2/(2h')} \xrightarrow[m \rightarrow \infty]{P} p(R)$. By the Continuous Mapping Theorem [26], we conclude that

$$\hat{p}_m(s, a|R) \xrightarrow[m \rightarrow \infty]{P} \frac{p(s, a, R)}{p(R)} = p(s, a|R).$$

□

The proof associated with Theorem 4.2 follows.

Proof. By Lemma 4.1, as $m \rightarrow \infty$, \hat{p}_m converges to the true likelihood, so we can adopt existing tools from Bayesian asymptotic theory.

We first define an equivalence relation on \mathcal{R} , denoted by \simeq :

$$R_1 \simeq R_2 \text{ iff } p(\cdot|R_1) = p(\cdot|R_2), \text{ a.e.}$$

Note that \simeq satisfies reflexivity, symmetry, and transitivity and is, therefore an equivalence relation. We denote the equivalence class by $[\cdot]$, that is, $[R] = \{R' : R' \simeq R\}$, and the quotient space is defined as $\tilde{\mathcal{R}} := \mathcal{R}/\simeq = \{[R] : R \in \mathcal{R}\}$. The corresponding canonical projection is denoted by $\pi : \mathcal{R} \rightarrow \tilde{\mathcal{R}}, R \mapsto [R]$. Then, the projection π induces a prior distribution on $\tilde{\mathcal{R}}$ denoted by $\tilde{\Pi}$: $\tilde{\Pi}(A) := \Pi(\pi^{-1}(A))$. Moreover, $\tilde{\mathcal{R}}$ admits a metric \tilde{d} :

$$\tilde{d}([R_1], [R_2]) := \|p(\cdot|R_1) - p(\cdot|R_2)\|_{L^1}.$$

Because this metric uses the L^1 norm, it satisfies symmetry and triangular inequality. Additionally, it is true that

$$\tilde{d}([R_1], [R_2]) = 0 \iff p(\cdot|R_1) = p(\cdot|R_2), \text{ a.e.} \iff R_1 \simeq R_2 \iff [R_1] = [R_2],$$

so \tilde{d} fulfills the identity of indiscernibles principle. As a result, \tilde{d} is a valid distance metric on $\tilde{\mathcal{R}}$.

Then consider the following Bayesian model:

$$(s, a)|[R] \simeq p(s, a|[R]), [R] \in \tilde{\mathcal{R}}, [R] \simeq \tilde{\Pi}.$$

This model is well-defined since $p(s, a|[R])$ is independent of the representative of $[R]$ by the definition of the equivalence class. Observe that $\text{KL}(R, R^*) = \text{KL}([R], [R^*])$ by the definition of the equivalence class. Then, let $A = \{[R] : \text{KL}([R], [R^*]) < \epsilon\} \subset \tilde{\mathcal{R}}$. We can define $\pi^{-1}(A) = \{R \in \mathcal{R} : \text{KL}(R, R^*) < \epsilon\} \subset \mathcal{R}$. As a result, $\tilde{\Pi}(\{[R] : \text{KL}([R], [R^*]) < \epsilon\}) = \Pi(\{R : \text{KL}(R, R^*) < \epsilon\}) > 0$ for any $\epsilon > 0$, that is, the KL support condition is satisfied. Moreover, the mapping $[R] \rightarrow p(\cdot|R)$ is one-to-one. Because the Bayesian model is parameterized by $[R]$ and we assume that \mathcal{R} is a compact set, by van der Vaart [44][Lemma 10.6] (Appendix H) there exist consistent tests as required in Schwartz's Theorem. Then, by Schwartz [39] (Appendix G), the posterior $\tilde{\Pi}_n$ on $\tilde{\mathcal{R}}$ is consistent. That is, for any $\epsilon > 0$, $\tilde{\Pi}_n(\{[R] : \tilde{d}([R], [R^*]) < \epsilon\}) \xrightarrow[n \rightarrow \infty]{m \rightarrow \infty} 1$. Put in terms of the original parameter space,

$$\Pi_m^n(\{R : \|p(\cdot|R) - p(\cdot|R^*)\|_{L^1} < \epsilon\}) = \tilde{\Pi}_m^n(\{[R] : \tilde{d}([R], [R^*]) < \epsilon\}) \xrightarrow[n \rightarrow \infty]{m \rightarrow \infty}, \forall \epsilon > 0.$$

□

E Asymptotic expansion of the mean integrated squared error Theorem 1

Theorem E.1. (i) The integrated squared bias of the kernel density estimator can be expanded as

$$ISB\{\hat{f}(\cdot; \mathbf{H})\} = \frac{1}{4} c_2(K)^2 \text{vec}^\top \mathbf{R} (D^{\otimes 2} f) (\text{vec } \mathbf{H})^{\otimes 2} + o(\|\text{vec } \mathbf{H}\|^2). \quad (9)$$

(ii) The integrated variance of the kernel density estimator can be expanded as

$$IV\{\hat{f}(\cdot; \mathbf{H})\} = m^{-1} |\mathbf{H}|^{-1/2} R(K) + o(m^{-1} |\mathbf{H}|^{-1/2}). \quad (10)$$

Algorithm 1 Kernel Density Bayesian IRL

-
- 1: **Input:** m training demonstration, n expert demonstrations, # MCMC iterations c
 - 2: **for** $l = 1, \dots, c$ **do**
 - 3: Sample a reward function \tilde{R}_l from the posterior distribution (Equation 6, main paper)
 - 4: Update the density function of the posterior \hat{p}_m^n using Equation 5 (main paper)
 - 5: **end for**
 - 6: **Output:** all sampled reward functions $\{R_l\}_{l=1}^c$
-

Here, \hat{f} is the estimated density function, \mathbf{H} is a matrix of bandwidth values, $c_2(K) = \int_{\mathcal{R}^d} z_i^2 K(z) dz$ for all $i = 1, \dots, d$ is the variance of the kernel function K , and m is the size of the training dataset. In our work, \mathbf{H} is a diagonal matrix where every element on the diagonal is the same bandwidth h_m . In this work, we assume that f is square-integrable and twice differentiable and that the bandwidth matrix $\mathbf{H} \rightarrow 0$ is $m \rightarrow \infty$. Because we use a Gaussian kernel for K , we know that it is square integrable, spherically symmetric, and has a finite second-order moment.

F Wand and Jones, Equation 4.16

The mean integrated squared error (MISE) of a multivariate kernel density estimator is defined as:

$$MISE\{\hat{f}(\cdot; \mathbf{H})\} = n^{-1}(4\pi)^{-\frac{d}{2}} |\mathbf{H}|^{-\frac{1}{2}} + w^\top \{(1 - n^{-1})\Omega_2 - 2\Omega_1 + \Omega_0\}w$$

where \mathbf{H} is a matrix of bandwidth values, n is the size of the dataset, Ω_a denotes the $k \times k$ matrix with (l, l') entry equal to $\phi_a \mathbf{H} + \Sigma_l + \Sigma_{l'}(\mu_l - \mu_{l'})$, ϕ_d is a d -variate Normal kernel, $w = (w_1, \dots, w_k)^\top$ is a vector of positive numbers summing to 1, and for each $l = 1, \dots, k$, μ_l is a $d \times 1$ vector and Σ_l is a $d \times d$ covariance matrix.

G Schwartz's Theorem

If $p_0 \in KL(\Pi)$ and for every neighborhood \mathcal{U} of p_0 there exist tests ϕ_n such that $P_0^n \phi_n \rightarrow 0$ and $\sup_{p \in \mathcal{U}^c} P^n(1 - \phi_n) \rightarrow 0$, then the posterior distribution $\Pi_n(\cdot | X_1, \dots, X_n)$ in the model $X_1, \dots, X_n | p \sim^{iid} p$ and $p \sim \Pi$ is strongly consistent at p_0 .

H Asymptotic Statistics, Lemma 10.6

Lemma H.1. Suppose that Θ is σ -compact, $P_\theta \neq P_{\theta'}$ for every pair $\theta \neq \theta'$, and the maps $\theta \rightarrow P_\theta$ are continuous for the total variation norm. Then there exists a sequence of estimators that is uniformly consistent on every compact subset of Θ .

Here, Θ is the space of parameters, P is the probability density function, and $\theta \in \Theta$ is a parameter.

I KD-BIRL algorithm

Algorithm 1 is the general version of the KD-BIRL algorithm where the expert demonstrations and training dataset are already available. A version of the algorithm that is suited for simulated datasets which require dataset generation can be seen in Algorithm 2.

J Calculating Expected Value Difference (EVD)

The procedure to calculate EVD varies depending on the method. For all methods, this process requires a set of reward samples. Because KD-BIRL and BIRL both use MCMC sampling, we can use the reward samples generated from each iteration. AVRIL does not use MCMC, so we have to modify the approach to generating samples depending on the structure of the reward function. When the reward function is a vector with length equal to the cardinality of the state space, we use the AVRIL agent to estimate the variational mean and standard deviation of reward at each state in the environment. Using these statistics, we then assume that the reward samples arise from a multivariate normal distribution and use numpy to generate samples according to the mean and standard deviation information collected. Once we have samples, we can then calculate EVD and 95% confidence intervals. Recall that EVD is

Algorithm 2 Kernel Density Bayesian IRL in a simulated Environment

```

1: Input: MDP  $M$ ,  $k$ ,  $m$ ,  $n$ , true reward  $R^*$ , # MCMC iterations  $c$ 
2: Generate  $k$  reward functions  $R_1 \dots, R_k \sim u$ .
3: for  $q = 1, \dots, k$  do ▷ Generate training data
4:    $\pi_q := \text{PolicyIteration}(M, R_q)$ 
5:   Generate  $\lfloor m/k \rfloor$  demonstrations using agent  $\pi_q$ 
6: end for
7:  $\pi_{opt} := \text{PolicyIteration}(M, R^*)$ 
8: Generate  $n$  demonstrations using agent  $\pi_{opt}$  ▷ Generate expert data
9: for  $l = 1, \dots, c$  do
10:   Sample a reward function  $\tilde{R}_l$  from the posterior distribution (Equation 6, main paper)
11:   Update the density function of the posterior  $\hat{p}_m^n$  using Equation 5 (main paper)
12: end for
13: Output: all sampled reward functions  $\{R_l\}_{l=1}^c$ 

```

defined as $|V^*(r^A) - V^{\pi^*(r^L)}(r^A)|$ where r^A is the ground truth known reward and r^L is the learned reward. For a given method, we calculate 95% confidence intervals across the EVD for each of the reward samples. Given a reward sample, we can calculate EVD, where r^L is the sample, and r^A is the known reward. To determine the value of the policy optimizing for a particular reward function, we train an optimal agent for that reward function, and generate demonstrations characterizing its behavior; the value is then the average reward received across those demonstrations. Finally, we calculate the difference between the value of the policy for r^A and r^L , and report confidence intervals across these values for all samples for a given method.

In the Sepsis environment, we use two methods of reward function featurization. In both, because the reward function does not consider individual discretized states, we cannot use the earlier approach to calculate EVD for AVRIL. To generate EVDs, we used the trained AVRIL agent to generate trajectories using agent-recommended actions starting from an initial state; the EVD here is the difference between the total value of these trajectories and the total value of trajectories generated using the correct reward function (independent of AVRIL).

K Choosing bandwidth hyperparameters for KD-BIRL

Now, we investigate the effect of the bandwidth hyperparameters h and h' on KD-BIRL's posterior distribution for the reward function $R^* = [0, 0, 0, 1]$, marginalized at state $[1, 1]$ (Figure 6). Recall that h and h' correspond to the bandwidth for the state-action pairs and reward functions, respectively. Note that the density of reward samples varies more with h' than h , but it is important to tune both these hyperparameters because the resulting posterior distributions can change substantially.

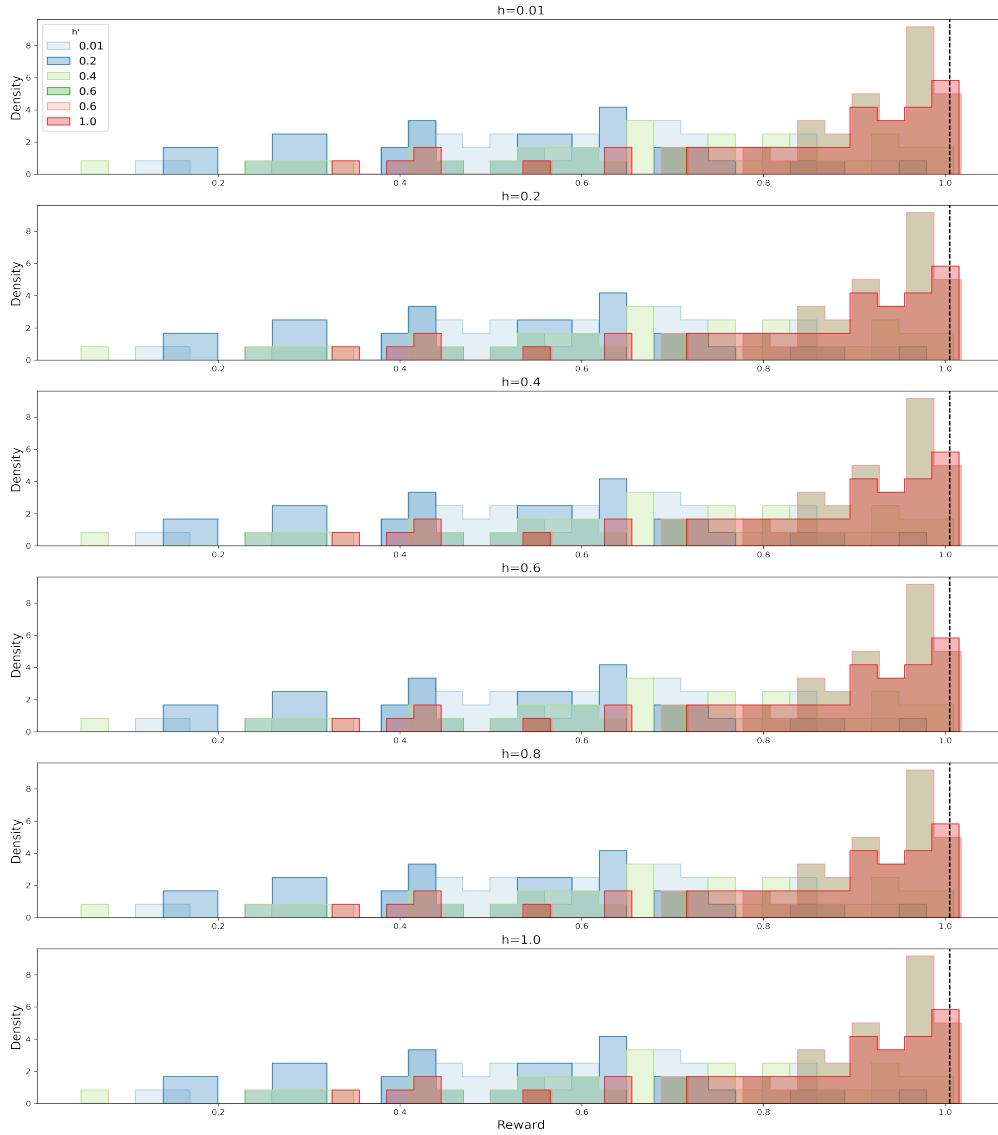


Figure 6: Density plots of the KD-BIRL posterior distributions for the reward function $R^* = [0, 0, 0, 1]$ when varying bandwidth hyperparameters, marginalized at state $[1, 1]$. We vary h and h' , two hyperparameters that correspond to the bandwidth for the state-action pairs and reward functions.

L Sepsis Environment

The Sepsis environment is a simulation setting that models Sepsis treatment. There are 48 state features(Appendix L) in the original environment, comprised of 46 physiological covariates and an action and state index.

Feature	Description
Albumin	Measured value of Albumin, a protein made by the liver
Anion Gap	Measured difference between the negatively and positively charged electrolytes in blood
Bands	Measuring band neutrophil concentration
Bicarbonate	Measured arterial blood gas
Bilirubin	Measured bilirubin
BUN	Measured Blood Urea Nitrogen
Chloride	Measured chloride
Creatinine	Measured Creatinine
DiasBP	Diastolic blood pressure
Glucose	Administered glucose
Glucose	Measured glucose
Heart Rate	Measured Heart Rate
Hematocrit	Measure of the proportion of red blood cells
Hemoglobin	Measured hemoglobin
INR	International normalized ratio
Lactate	Measured lactate
MeanBP	Mean Blood Pressure
PaCO2	Partial pressure of Carbon Dioxide
Platelet	Measured platelet count
Potassium	Measured potassium
PT	Prothrombin time
RespRate	Respiratory rate
Sodium	Measured sodium
SpO2	Measured oxygen saturation
SysBP	Measured systolic blood pressure
TempC	Temperature in degrees Celsius
WBC	White blood cell count
age	Age in years
is male	Gender, true or false
race	Ethnicity (white, black, hispanic or other)
height	Height in inches
Weight	Weight in kgs
Vent	Patient is on ventilator
SOFA	Sepsis related organ failure score
LODS	Logistic organ disfunction score
SIRS	Systemic inflammatory response syndrome
qSOFA	Quick SOFA score
qSOFA Sysbp Score	Quick SOFA that incorporates systolic blood pressure measurement
qSOFA GCS Score	Quick SOFA incorporating Glasgow Coma Scale
qSofa Respirate Score	Quick SOFA incorporating respiratory rate
Elixhauser hospital	Hospital uses Elixhauser comorbidity software
Blood culture positive	Bacteria is present in the blood

The original Sepsis environment uses the features described in Appendix L to represent the patient state. In the first method of featurization we consider in our experiments, we consider only three features that directly affect the reward received in a given state. These are SOFA, qSOFA, and qSOFA Sysbp Score. Intuitively, these can be thought of as features of the state that are most relevant to the reward function. In the second method of featurization, we consider all of the state features as well as the action chosen, and use a variational auto-encoder to generate a low dimensional representation.